Amino acid based stabilization of oxide nanocrystals in polar media: from insight in ligand exchange to solution ^{1}H NMR probing of short–chained adsorbates

Jonathan De Roo,[*,†,‡,¶] Sofie Coucke,[†,‡,¶] Hannes Rijckaert,[†] Katrien De Keukeleere,[†] Davy Sinnaeve,[¶] Zeger Hens,[‡,§] José C. Martins,[¶] and Isabel Van Driessche[*,†]

Sol-gel Center for Research on Inorganic Powders and Thin films Synthesis (SCRiPTS), Ghent University, Ghent, Belgium, Physics and Chemistry of Nanostructures group (PCN), Ghent University, Ghent, Belgium, NMR and Structure Analysis Unit (NMRSTR), Ghent University, Ghent, Belgium, and Center for Nano and Biophotonics, Ghent University, Ghent, Belgium

E-mail: Jonathan.DeRoo@ugent.be; Isabel.VanDriessche@ugent.be

KEYWORDS: surface chemistry, nanocomposite

[*]To whom correspondence should be addressed
[†]SCRiPTS, Ghent University
[‡]PCN, Ghent University
[¶]NMR group, Ghent University
[§]Photonics group, Ghent University

Abstract

Ligand exchange is a crucial step between nanocrystal synthesis and nanocrystal application. Although colloidal stability and ligand exchange in nonpolar media is readily established, the exchange of native, hydrophobic ligands with polar ligands is less systematic. In this paper, we present a versatile ligand exchange strategy for the phase transfer of carboxylic acid capped HfO_2 and ZrO_2 nanocrystals to various polar solvents, based on small amino acids as the incoming ligand. To gain insight in the fundamental mechanism of the exchange, we study this system with a combination of FTIR, zeta potential measurements and solution ^{1}H NMR techniques. The detection of surface–associated, small ligands with solution NMR proves challenging in this respect. Tightly bound amino acids are undetectable but their existence can be proven through displacement with other ligands in titration experiments. Alternatively, we find that methyl moieties belonging to bound species can circumvent these limitations because of their more favorable relaxation properties as a result of internal mobility.

Introduction

The emergence of nanocrystals (NCs) has provided material science with extremely versatile building blocks with regard to size, shape, chemical composition and crystal structure.[1] The NC surface is an indispensable part of these building blocks since its composition determines colloidal stability in various solvents and influences the nanocrystal's physical and chemical properties. However, with its typical capping of hydrophobic ligands, the surface composition of as–synthesized nanocrystals is ill–suited for applications that require solubility in polar solvents,[2] complete ligand removal,[3] or subtle doping of the surface.[4] This applies in particular to the formation of all–inorganic nanocomposites, comprising a matrix and nanoscale inclusions, for which NCs, soluble in polar solvents, are typically needed. Examples include (i) capacitor[5] or superconducting[6,7] nanocomposite thin films formed using a methanol–based precursor solution containing both molecular precursors for the matrix and dispersed metal oxide NCs (ii) nanocrystal–in–glass composites, fabricated from aqueous dispersions of indium tin oxide[8] or (iii) mesoporous mate-

rials, constructed from NC building blocks by electrostatic interaction with a structure directing block–copolymer.[9]

De–aggregation of NCs in nonpolar solvents is often attained by providing a steric stabilizer.[10–14] In order to achieve colloidal stability in polar solvents, the hydrophobic, steric ligands need to be exchanged for organic or inorganic polar ligands. Several strategies have already been developed to transfer metal, metal selenide and metal sulfide NCs to polar solvents, yet these exchange schemes cannot be simply transferred to metal oxide NCs. Sulfide or selenide based ligands for example, proved excellent for ligand exchange on metals and metal sulfides, selenides, phosphides or arsenides but showed little affinity towards oxide NCs.[15–22] In addition, ligand exchange schemes[19,23–25] tend to use solvents with high dielectric constants (e.g., formamide, $\varepsilon = 111$ or N-methylformamide, $\varepsilon = 180$) that favor electrostatic stabilization. However, the application of those high–boiling, unstable and toxic solvents is limited. Furthermore, most accounts in literature describe procedures providing electrostatic stabilization in basic conditions, and with negatively charged surfaces.[16–19,21,23,24,26–29] The formation of nanocomposites however, may involve acidic matrix precursor solutions[6,7] whereas the uptake of nanoparticles by immune cells was found to be enhanced by positive surface charges.[30] Potentially useful procedures in this respect involve the use of stripping agents such as $NOBF_4$,[31] RO_3BF_4,[32] and BF_3[33] which operate in acidic conditions, or dopamine, which stabilizes titania NCs by a positive surface charge.[34] The former approach however, does not lead to long term stable dispersions whereas dopamine is an important neurotransmitter, involved in addictive behavior, and therefore a restricted chemical. Also amino acids are known to stabilize NCs in water,[35–38] but no ligand exchange process took place in those examples as the NCs were synthesized in the water phase with the amino acids already present.

Here, we present a new ligand exchange strategy to transfer metal oxide nanocrystals capped with apolar ligands to a variety of common polar solvents. The method is based upon exposure of metal oxide NCs to short–chain amino acids under acidic conditions, implying that it does not introduce additional metal ions to the dispersion and uses reagents that are all perfectly stable in air and moisture. Using mostly hafnium oxide as a metal oxide NC model system with a

well–understood surface chemistry[10,39] — and potentially useful as luminescence host,[40] as dielectric[41,42] or for medical applications,[43] — we can elucidate the ligand exchange mechanism through a combination of FTIR, zeta potential measurements and solution ^{1}H NMR techniques. The latter is especially popular to probe the dynamic behavior of ligands *in situ* in solution and is mostly used to characterize NCs in apolar media, stabilized by long, steric ligands.[10,39,44–48] Having available metal oxide NCs stabilized by various amino acids however, enables us to explore the possibilities of the technique for the detection of short–chain adsorbates that only have protons close to the nanocrystal surface. While the resonances of these protons are typically broadened beyond detection,[39] we show that *in situ* titration experiments with competing ligands allow the observation of the released ligands. Moreover, we found that surface–bound amino acids featuring methyl moieties are directly discernable in the ^{1}H NMR spectrum due to the latter's internal mobility. The methodology presented in this work to characterize small ligands bound to NC surfaces, here amino acids and metal oxides, can be regarded as general and equally applicable for any type of NC and ligand.

Experimental

HfO_2 and ZrO_2 NCs were synthesized according to a microwave-assisted benzyl alcohol synthesis.[49,50] Briefly, 0.13 g of the metal chloride was dissolved in 0.5 mL dibenzylether and 4 mL benzyl alcohol, and heated at 220 °C in the microwave. After synthesis, the NCs were stabilized in 4 mL chloroform by a post synthetic surface functionalization with dodecanoic acid (DDAc).[10] The particles were washed three times with acetone. The HfO_2 concentration was determined by drying one mL of suspension and by weighing the residue. The amount of organics was determined by TGA and subtracted from the weight of the residue. The concentration of the HfO_2 NC suspension was 0.06 M in hafnium (12.6 mg/mL).

In a typical ligand exchange, 1 mL of the HfO_2 or ZrO_2 dispersion was precipitated with acetone and centrifuged. Then 0.4 mmol trifluoroacetic acid (TFA) in 1 mL of methanol was added

(together with 0.05 mmol of amino acid, typically glutamine). After 30 min sonication, a clear suspension was obtained. The NCs were precipitated with toluene, to remove excess of ligands, and redispersed in methanol, acetone, butanol, ethanol, DMSO, isopropanol or acetonitrile. In some cases it might be necessary to add again 0.1 mmol TFA to obtain a stable dispersion. To determine the NC concentration, the suspension was again dried and measured in TGA. Typically, a weight loss of 12 – 15 % is associated with glutamine based samples and the final concentration is 0.045 M. The exchange reaction has thus a yield of 75 % and the losses are accounted for by the washing steps.

General characterization: For Dynamic Light Scattering (DLS) and zeta potential measurements a Malvern Nano ZS was used in backscattering mode (173 °). To calculate the zeta potential from the electrophoretic mobility, the Hückel approximation was applied. For X-ray Diffraction (XRD) characterization a Thermo Scientific ARL X'tra X–ray diffractometer was used with the CuKα line as the primary source. For infrared measurements a Perkin Elmer FT–IR spectrometer spectrum 1000, equiped with a HATR module was used.

NMR characterization: NC suspensions were evaporated with N_2 and redissolved in toluene-d_8. Nuclear Magnetic Resonance (NMR) measurements were recorded on a Bruker Avance II spectrometer operating at a ^{1}H frequency of 500.13 MHz and equipped with a ^{1}H, ^{13}C, ^{31}P TXI–Z probe, or on a Bruker Avance III spectrometer operating at the same ^{1}H frequency and equipped with a BBI–Z probe. The sample temperature was set to 298.2 K throughout. One–dimensional (1D) ^{1}H and 2D NOESY (Nuclear Overhauser Effect SpectroscopY) spectra were acquired using standard pulse sequences from the Bruker library. For the quantitative 1D ^{1}H measurements, 64k time domain points were sampled with the spectral width set to 16 ppm and a relaxation delay of 30 s. For the NOESY, the mixing time was 300 ms, while 4096 time domain points in the direct dimension and 512 time domain points in the indirect dimension were acquired, with the spectral width in both dimensions set to 16 ppm. In some cases (supporting information), a zero–quantum cross–peak suppression was performed during the mixing time of the NOESY, using a swept–frequency 180 degree pulse and a gradient pulse applied simultaneously, as described by

Thrippleton and Keeler.[51] For 2D processing, the acquired time domain data was multiplied with a squared cosine bell function in both dimensions and zero filled until a 4096×1024 real data matrix. The 1D spectra were multiplied with an exponential window function with a line–broadening factor of 0.3. Ligand concentrations were measured using the Digital ERETIC method implemented in Topspin 3.1. In this method the integration of a resonance belonging to the ligand is compared to the integration of a resonance in a standard sample with a known concentration. The error on the analysis is typically about 10 %. Diffusion measurements (2D DOSY) were performed using a double stimulated echo sequence for convection compensation and with monopolar gradient pulses.[52] Smoothed rectangle gradient pulse shapes were used throughout. The diffusion decay was sampled in 32 or 64 equal steps of squared gradient strength, ranging from 2% to 95% of the probe's maximum attainable value (calibrated at 50.2 G/cm). The gradient pulse duration and diffusion delay were optimized to ensure an attenuation of the signal in the final increment of less than 10 % relative to the first increment. The diffusion coefficients were obtained by fitting the appropriate Stejskal–Tanner equation to the signal intensity decay.[53]

Results and discussion

Phase transfer with and without amino acids

Dodecanoic acid capped HfO_2 NCs, dispersed in chloroform, were synthesized using established procedures.[10,49] Dodecanoic acid is dissociatively adsorbed on the HfO_2 NC surface (Figure 1A), a binding motif classified as $NC(X)_2$.[39] Since it was already shown that ligand exchange processes with carboxylic acids are governed by acidity[4,10,54,55] and that it proved possible to transfer $NaYF_4$ NCs to water by simple protonation of the original oleate ligand,[55] we sought to transfer the HfO_2 NCs to methanol using the same principle. The HfO_2 NCs were precipitated with acetone and a methanol solution of trifluorosulphonic acid (TFSA) was added. However, even after prolonged ultrasound treatment the dispersion remained turbid and unstable. Interestingly, a similar treatment with trifluoroacetic acid (TFA), another strong organic acid, did result in a transparent dispersion.

Dynamic Light Scattering (DLS) measurements confirmed that the solvodynamic radius in chloroform and methanol were similar (Figure 1B). These TFA stabilized HfO_2 NCs showed a zeta potential of -22 mV (Figure S1), while the pH of the methanolic dispersion was -0.04. A negative zeta potential implies that there must be more negatively charged species adsorbed on the surface than positively charged ones. Although the solution is very acidic, the adsorption of trifluoroacetate anions (TFA^-) thus appears to be preferred over the adsorption of protons (Figure 1A, route A). A negative zeta potential at such low pH values is remarkable and has — to our knowledge — never been reported. We rationalize that the differences between TFSA and TFA are due to their differences in acidity and nucleophilicity. TFA has a pKa in water of -0.3 while TFSA has a pKa of -12. TFSA is therefore classified as a superacid, thus possessing negligible nucleophilic properties, and does not bind to the NC surface. It is worth mentioning that the NCs are unaltered by the harsh pH conditions during the exchange, as demonstrated by their X–ray diffractograms before and after exchange (Figure S2).

Unfortunately, the TFA stabilized HfO_2 NCs are not colloidally stable, neither upon dilution nor over a longer period of time (a few weeks). In addition, the NCs cannot be precipitated by the addition of apolar solvents such as toluene (the dispersion remains stable), so that purification of the NCs is problematic. These issues could be readily solved by the addition of glutamine (Gln) to the NC dispersion. The HfO_2 NCs were subsequently precipitated with toluene and redispersed in methanol. As attested by DLS, the solvodynamic diameter remains the same (Figure 1B). The dispersion in methanol is colorless, optically fully transparent (inset in Figure 1B) and remains colloidally stable for at least 1 year (Figure S3). The impact of Gln on the NC surface chemistry is also clearly reflected in the changes in zeta potential to $+26$ mV (Figure S1). A pH of 1.92 was measured and since the tabulated pKa values of Gln are 2.17 and 9.31, most of the Gln is present as positively charged, fully protonated species. The positive zeta potential of the NCs thus most likely results from positively charged Gln^+ molecules adsorbed on the surface (Figure 1A, Route B).

In order to further compare the HfO_2 dispersions, formed with and without Gln, both suspen-

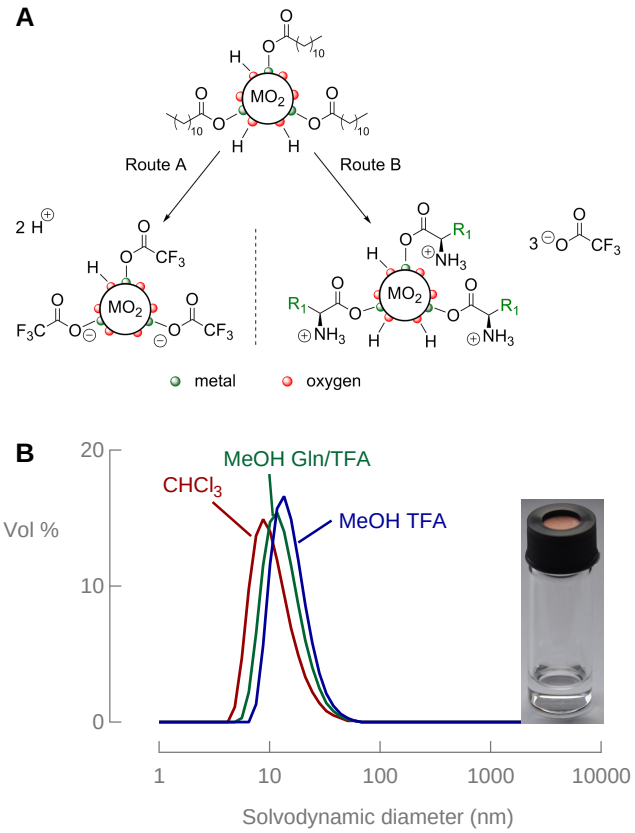

Figure 1: (A) Surface chemistry models representing the various ligand exchange strategies, starting from dodecanoic acid capped metal oxide NCs. In route A, the NCs are treated with trifluoroacetic acid (TFA). In route B, the NCs are treated with TFA and glutamine (Gln). The stoichiometric relationships during the exchange are unknown and are shown here as arbitrary. Note that all charges are balanced. (B) DLS measurements of HfO_2 NCs in chloroform with dodecanoic acid or in methanol with TFA and/or glutamine Gln. The inset displays a dispersion of HfO_2 NCs with Gln and TFA.

sions were dried during 24 hours in an oven at 60 °C. The subsequently measured IR spectra both clearly feature the characteristic absorption bands of C–F stretches (Figure 2), confirming the presence of TFA in both samples. Since TFA is volatile and a drying step was performed, it can be excluded that these stretches are from unbound TFA. The first spectrum confirms that TFA is directly adsorbed (dissociatively) to the HfO_2 NC surface, while the second spectrum demonstrates that the trifluoroacetate acts as a counterion for the positively charged Gln that is adsorbed on the HfO_2 NC surface (Figure 1A, Route B). Further experimental support for this surface chemistry is found in the phase transfer to methanol, which proceeds with the combination of Gln and TFSA (Figure S4) but not with Gln alone. We infer respectively that Gln may be protonated by any strong organic acid and that the zwitterionic form of Gln is unable to provide electrostatic stabilization.

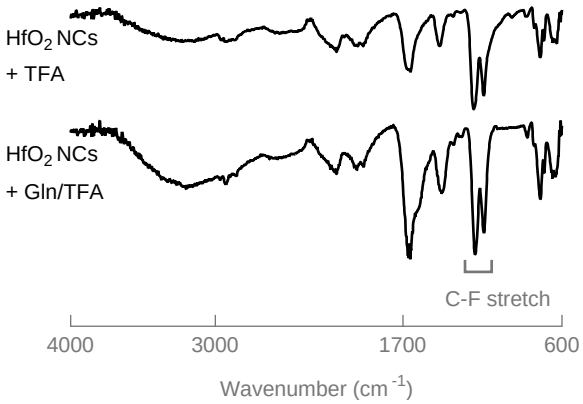

Figure 2: The IR spectra after evaporation of a purified HfO_2 suspension, either stabilized with TFA alone or with TFA and Gln.

The above results led to a general procedure to transfer carboxylic acid capped metal oxide NCs from apolar to polar solvents, see Figure 3A. After precipitation of the NCs with acetone, centrifugation and decantation, we added a methanolic solution of a strong organic acid and an amino acid. For purification purposes, the NCs are precipitated with toluene and could be redispersed in either methanol or various other polar solvents, showing the versatility of the approach (Figure 3B). We have verified the ligand exchange and phase transfer of HfO_2 and ZrO_2[50] NCs, initially dispersed in chloroform or toluene, using most amino acids: lysine, glutamine, glycine, serine, arginine, aspartic acid, histidine, leucine, methionine, threonine, asparagine and glutamic

acid (Figure S5). The choice of a specific amino acid has an influence on the surface charge, as reflected by the variation in zeta potential, *e.g.*, glutamine (+26 mV), lysine with an extra amine group in the side chain (+ 45 mV) or leucine, an amino acid with a nonpolar side–chain (+ 5 mV), see Figure S1. Such differences might play a role in the interaction with structure directing agents in the synthesis of mesoporous materials.[9] In addition, most amino acids contain only C, H, O and N, which burn off easily, and do not introduce new elements in, *e.g.*, a nanocomposite of the high temperature superconductor $YBa_2Cu_3O_{7-\delta}$.[7]

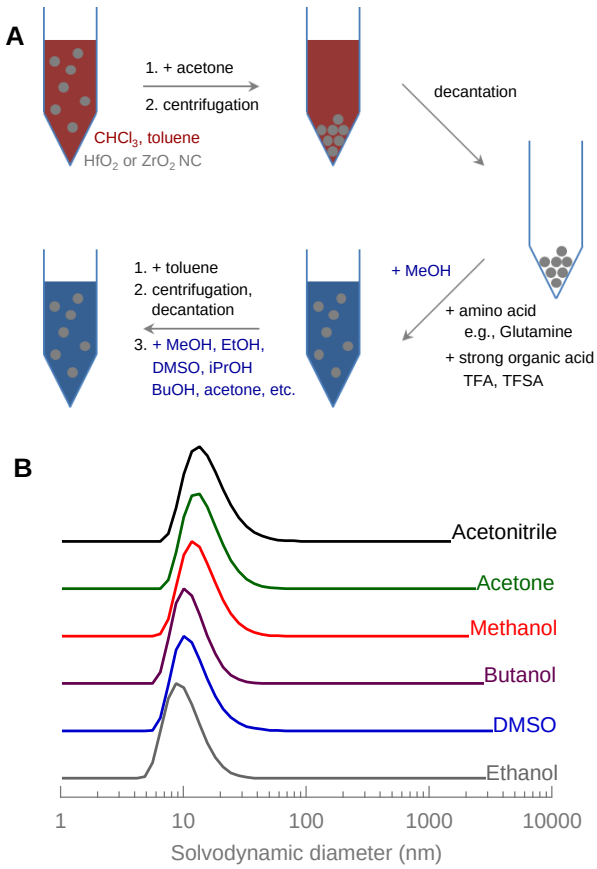

Figure 3: (A) Schematic overview of the NC phase transfer from apolar solvents to various polar solvents with amino acids. The colors are to guide the eye and are no reference to the real color of the suspension. (B) DLS measurements of HfO_2 NCs stabilized with TFA and Gln in various polar solvents.

^{1}H NMR characterization of the surface after phase transfer

Focusing on Gln/TFA stabilized HfO_2 NCs in methanol, the positive zeta potential of the HfO_2 NCs already suggested that Gln is directly bound to the NC surface. However, this is an indirect deduction and does not give any information about the fate of the original ligand, dodecanoic acid (DDAc). Therefore, we used the ^{1}H solution NMR toolbox that was specifically developed to study the organic–inorganic interface of NC ligand shells, albeit mostly applied to bulky ligands in apolar solvents.[56]

In the ^{1}H NMR spectrum of glutamine stabilized HfO_2 NCs, obtained after phase transfer to methanol (Figure 4A), resonances of both DDAc (the original ligand) and Gln (the new ligand) are recognized. The DDAc resonances (except **a** and **b**) comprise two components, characterized by sharp and broad resonances respectively, superimposed on each other (Figure 4A). Sharp resonances, with resolved multiplet structures, are typical for solvated small molecules. In contrast, bound ligands lead to broad ^{1}H signals due slower molecular tumbling and thus a decreased T_2 relaxation time constant.[56] This broadening is the most severe for protons close to the NC surface, explaining why the bound **a** and **b** resonances are broadened beyond detection, while the protons further away increasingly benefit from internal molecular motional freedom. The set of broad DDAc resonances are therefore assigned to bound DDAc molecules. As the broad and sharp signals of resonances **c** and **d** overlap, the bound fraction was determined by deconvolution. Finally, a ligand density of 0.3 DDAc nm^{-2} was determined. As the ligand density was 3.6 nm^{-2} before ligand exchange, 92 % of the original ligand was thus removed from the surface. We infer that the remaining 8 % of DDAc ligands provide a steric contribution to the colloidal stabilization of the NCs, in addition to the electrostatic contribution provided by glutamine.

The bound state of DDAc was confirmed by DOSY and NOESY NMR techniques. Using a bi–exponential fitting of the DOSY spectra, diffusion coefficients of 64 $\pm$ 3 μm^2/s and 986 $\pm$ 20 μm^2/s were obtained for the bound and free DDAc respectively. Using the Stokes–Einstein equation, the diffusion coefficient of bound DDAc corresponds to a solvodynamic diameter (d_s) of 12.5 nm. Since this is the same diameter as in the DLS analysis, these broad DDAC signals can

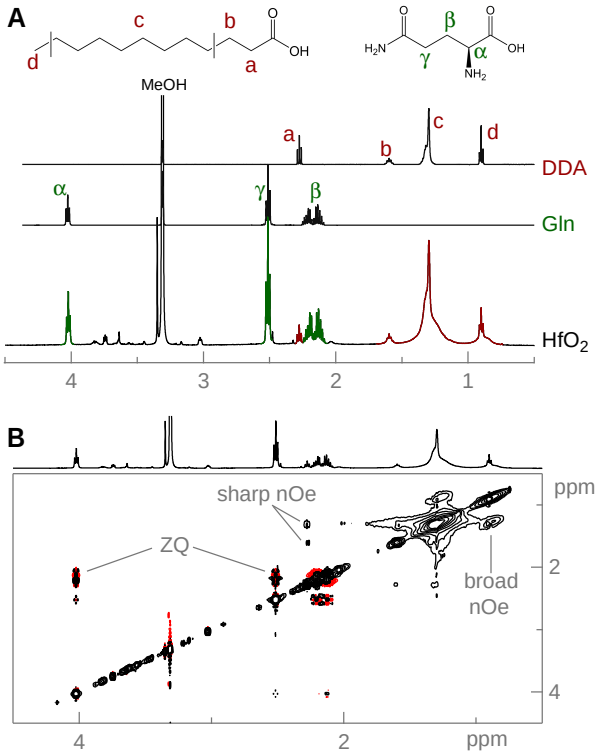

Figure 4: (A) In the ^{1}H NMR spectrum of HfO_2 in MeOD-d_4, stabilized with Gln and TFA and purified by precipitation with toluene, both sharp and broad resonances of DDAc are present, while only sharp Gln signals are visible. Also the reference spectra of Gln and DDAc are presented. (B) In the 2D NOESY spectrum of the same suspension, nOe cross–peaks, mutually connecting either sharp resonances or broad resonances, are present for DDAc. For Gln, only zero–quantum (ZQ) cross–peaks are visible.

be attributed to tightly bound ligands. Additional support is provided by the negative (black) nOe cross peaks between the resonances of bound DDAc in the NOESY spectrum (Figure 4B), a typical feature of bound ligands.[56] Interestingly, the nOe cross peaks between the sharp resonances (**a** – **b** and **a** – **c**) of 'free' DDAc also possess a negative sign. This is known to result from a so–called transfer nOe effect, resulting from fast exchange of ligands between a bound state and a more populated free, solvated state.[57] The line width is a weight average and thus dominated by the free fraction while the nOe effect that rapidly develops when in the bound state prevails in the overall exchange averaged NOESY spectrum. A similar behavior was observed before in toluene for oleic acid, where it was concluded that there are three possible ligand states: free, bound and weakly entangled in the ligand shell.[58] We reason that the same situation applies here for DDAc, binding to HfO_2 NCs in methanol.

The resonances of Gln, however, are sharp (Figure 4A) and no slowly diffusing species related to glutamine is detected in the DOSY spectrum. In addition, negative (transfer) nOe cross peaks are absent in the NOESY spectrum. Only zero–quantum coherence (ZQ) cross–peaks are visible (Figure 4B), resulting from mutual ^{1}H–^{1}H scalar coupling interaction. It is also worth mentioning that the Gln concentration is rather low: 3 mM or 3 % of the original amount of Gln, indicating that most of the glutamine is removed during the purification step (precipitation of the NCs with toluene and resuspension in methanol). Indeed, the supernatant contains a high concentration of glutamine, next to dodecanoic acid (Figure S6). Other amino acids, *e.g.*, lysine, asparagine, *etc.* show the same behavior, *i.e.*, their resonances feature no line broadening, no negative (transfer) nOe cross peaks and correspond to fast diffusing species. However, we inferred from the first section that the amino acids should be bound to NC surface and therefore, we suggest that the established NMR toolbox[56] is unable to prove ligand binding in this case, providing a false negative result.

Competitive titration as a workaround for line broadening

A possible explanation for the lack of evidence for bound Gln in the ^{1}H NMR spectrum could be that, the bound Gln resonances are broadend beyond detection as the Gln molecules feature insuf-

ficient internal molecular motion to counter the efficient T_2 relaxation caused by slow molecular tumbling, in the same way as for the **a** and **b** resonances of DDAc. We explored techniques such as HRMAS (to eliminate magnetic susceptibility line broadening) or measurements at elevated temperatures in DMSO (90 °C, to increase internal, rotational mobility) to reduce the line width of the bound fraction and directly observe it, but to no avail. Finally, we were able to indirectly prove the presence of bound Gln by gradually adding another amino acid (glycine, Gly), to a HfO_2 NC suspension, stabilized in MeOD–d_4 with TFA and Gln and purified with toluene. We expected Gly to compete with Gln for surface binding, thus gradually releasing Gln from the surface, see Figure 5A. Note that there is no reason to assume a significantly different binding strength of Gly to HfO_2 than Gln, since the side chain is expected to have only a small influence in this respect. This titration experiment is thus solely based on a stochastic redistribution of ligands on binding sites, *i.e.*, it is the higher concentration of Gly that will drive Gln from the surface.

In the experiment, we monitored the DDAc, Gln and Gly resonances and in each titration step, 0.56 μmol glycine was added to the HfO_2 NC suspension, see Figure 5B. Throughout the titration, the detected amount of free Gln increased, confirming that Gln was detaching from the surface. In addition, in the first three titration steps, the differential increase in Gly (Δn, as observed in NMR) does not match the amount of Gly that was added in each titration step (Figure 5B). We thus conclude that Gly also binds to the surface, where it is undetectable, replacing and releasing glutamine in the process. In addition, the fraction of bound DDAc (against the total amount of DDA) decreases, from 77 % to 56 %, probably also due to the competitive ligand binding with Gly.

A similar competitive titration was be performed on HfO_2 NCs, stabilized with only TFA in methanol, see Figure 6A. To this highly acidic solution (pH = - 0.04), 6.5 μmol Gln was added in each titration step, resulting in an increase of the bound DDAc fraction (Figure 6B). Although it seems counterintuitive that adding a competing ligand promotes DDAc binding, we note that the addition of Gln also increases the pH of the solution, resulting in a shift of the equilibrium between free and bound DDAc. On the other hand, in the first titration step, the increase in Gln

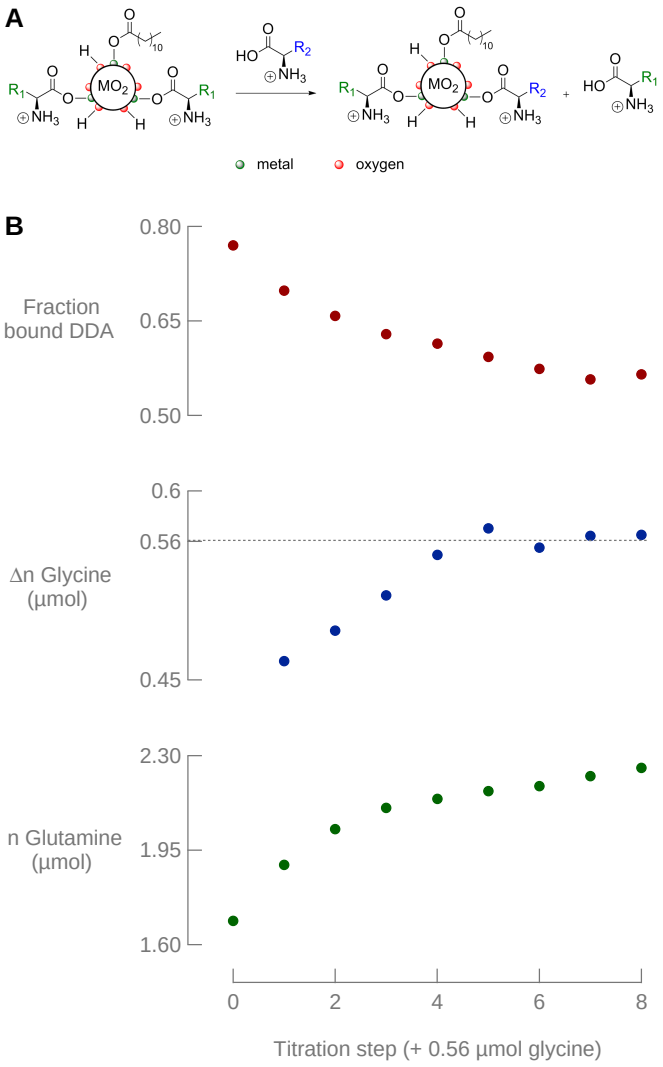

Figure 5: (A) General scheme of competitive titration. The addition of glycine (R_2 = H) in steps of 0.56 μmol drives bound glutamine ($R_1 = CH_2CH_2CONH_2$) from the surface into the solution as a free molecule. Note that the NC–ligand entity is positively charged. (B) The fraction bound DDAc (with respect to the total amount of DDAc) decreases during the titration with Gly. The amount n of observed free Gln increases, but the differential increase Δn of observed free Gly is lower than 0.56 μmol in the first titration steps.

intensity (Δn) was smaller than expected from the added Gln amount (Figure 6B), demonstrating the binding event of glutamine. From this deficiency, the ligand density for Gln was determined at 1 nm^{-2}. More information about the calculation of ligang densities is provided in the supporting information.

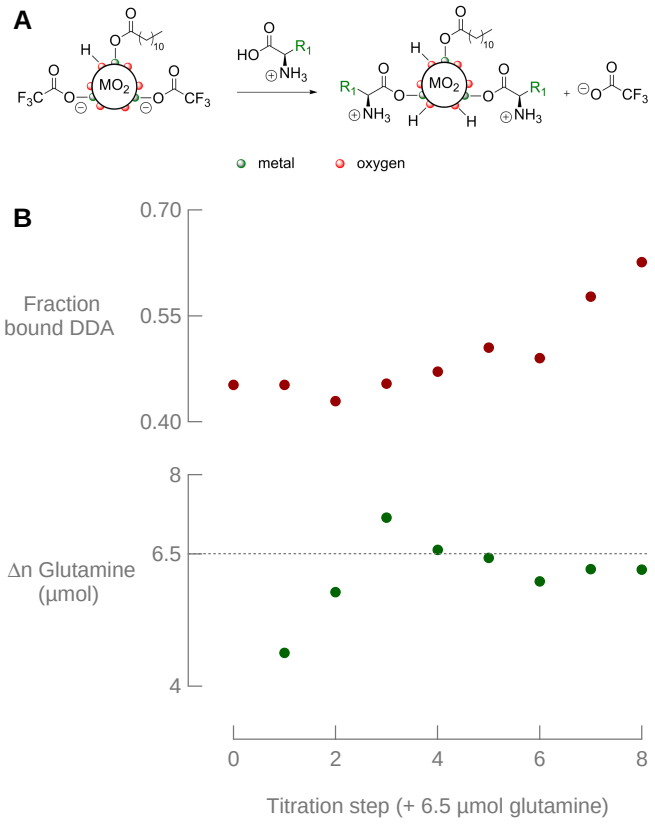

Figure 6: (A) When Gln (R_1 = $CH_2CH_2CONH_2$) is added to HfO_2 NCs, stabilized with TFA, Gln will replace TFA on the surface. Note that the NC–ligand entity is negatively charged before Gln addition and positively charged after Gln addition. (B) The fraction of bound DDAc and the differential increase Δn of observed free Gln upon gradual addition (6.5 μmol per step) of Gln to TFA stabilized HfO_2 NCs in MeOD–d_4.

Methyl moieties in small, bound ligands are detectable.

The combination of the positive zeta potential and the competitive titration experiments has proven qualitatively and quantitatively that Gln is bound to the HfO_2 NCs. However, we could not directly detect a resonance of strongly bound Gln ligands in the ^{1}H NMR spectrum. Since the lack of

internal mobility close to the surface is the most important impediment, we postulated that methyl groups may afford a better chance to directly observe the bound ligands, as the rapid rotational motion of the methyl rotor should lead to increased T_2 relaxation time constants (Figure 7A). Therefore, we investigated leucine (Leu), methionine (Met) and threonine (Thr), each containing at least one methyl group, as amino acids in the ligand exchange. Whereas in the ^{1}H NMR spectrum, the methyl resonance of Thr and Leu overlaps with the alkyl resonances of DDAc (Figure S7), complicating spectral analysis, the methyl (δ) resonance of Met is situated in a different region than the DDAc resonances, although it overlaps with one of its own β resonances (Figure 7B). Upon close inspection of the spectrum, it can be seen that the signals around 2.1 ppm are a superposition of sharp β and δ signals from free, solvated Met, and a very broad contribution which we assign to the methyl (δ) resonance of bound Met (Figure 7B, indicated in green). Unfortunately, this is the only observable resonance for the bound Met ligand, thus no negative intramolecular nOe's could be detected to support the bound character of this species. However, a negative intermolecular nOe cross–peak to the methylene resonances of the DDAc chain (δ–**c** in Figure 7C) is clearly visible, providing support that both species are simultaneously bound to the NC surface. A diffusion coefficient of 78 $\pm$ 10 μm^2/s measured on this broad δ resonance confirms its identity as tightly bound methionine, as this corresponds to a solvodynamic radius of 10.3 nm, and is very close to the diffusion coefficient of bound DDAc (63 $\pm$ 1 μm^2/s). We thus conclude that methyl units of tightly bound, small ligands can be detected and thus provide a probe to assess small ligand binding.

Having addressed the broad methyl resonance of bound Met, we turn to some additional interesting nOe cross–peaks between the sharp Met resonances. As for Gln, zero–quantum cross–peaks are visible between the scalarly coupled γ and β resonances or between the α and β resonances (Figure 7C). In contrast, between the uncoupled resonances α and γ of free Met, where no zero–quantum cross–peak is present, we can observe an intramolecular negative transfer nOe cross–peak, indicating some contribution of the entangled state in fast exchange with the free form (*vide supra*). This entangled state is also apparent from the sharp intermolecular negative cross–peak be-

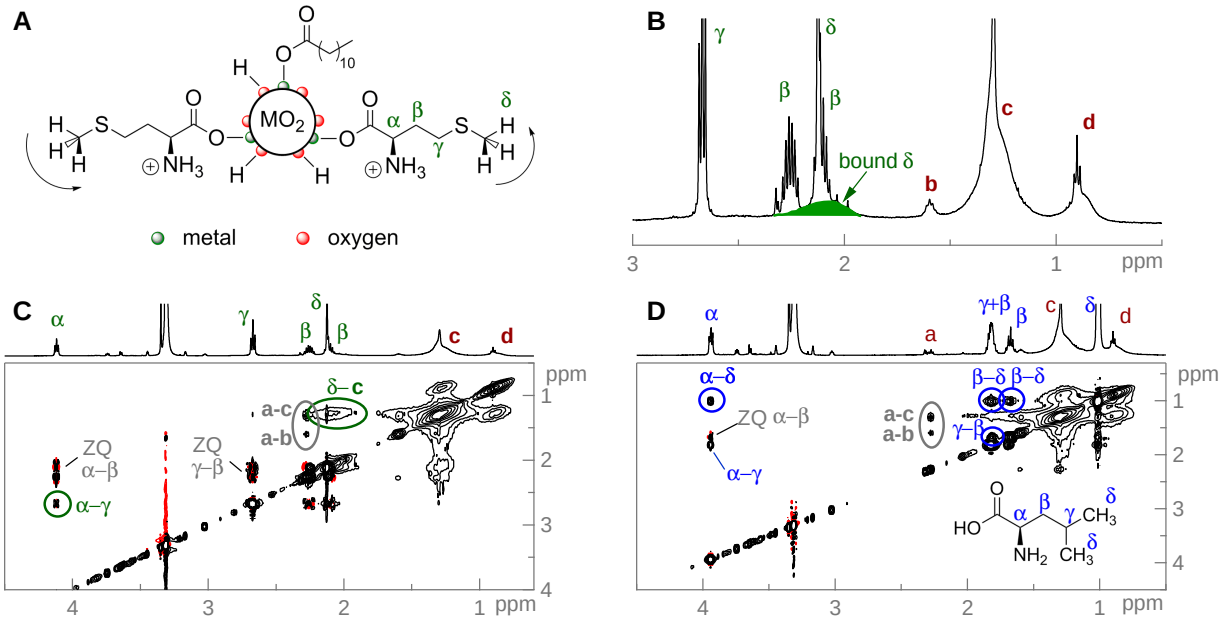

Figure 7: (A) HfO_2 NCs stabilized with methionine (Met). The methyl group possesses complete rotational freedom. (B) In the ^{1}H NMR spectrum of HfO_2 NCs with Met in MeOD-d_4, the broad resonance under the sharp δ resonance is assigned to the bound Met δ resonance (C) In the NOESY NMR spectrum of the same sample, a broad intermolecular nOe cross–peak is visible between the bound DDAc **c** resonance and the bound Met δ resonance. (D) The NOESY spectrum of HfO_2 NCs with Leu in MeOH-d_4.

tween δ and **c**, superimposed on the broad cross–peak (Figure 7C). Nevertheless, we infer that the entangled state is marginally populated, as the transfer nOe cross–peakss are weak. Similar observations are made in the NOESY spectrum of Leu (Figure 7D) or Thr (Figure S8) stabilized HfO_2 NCs. Although mostly intramolecular negative nOe cross–peaks are detected between uncoupled spins, their weak intensity is underscored by the fact that they do not outshine the zero–quantum artifacts between the scalarly coupled resonances. When special precautions are taken to suppress the zero quantum cross–peaks, negative transfer nOe cross peaks also become observable for the Gln stabilized HfO_2 NCs (Figure S9). We thus conclude that all amino acids display a similar behavior, *i.e.*, the metal oxide NCs are primarily stabilized by a layer of strongly bound amino acids and residual DDAc molecules. Even though there is indication for the free amino acid fraction to interact weakly with the NC surface or the ligand shell, this entangled state is far less populated than the entangled state of fatty acids[58] and therefore seems hardly relevant for the stabilization. This is not too suprising given the short chain length of these amino acids. This will considerably reduce van der Waals interactions within the ligand shell.

Finally, we would like to emphasize that the above ligand binding assessments were only possible through the combination of three NMR techniques: 1D ^{1}H, 2D NOESY and 2D DOSY. Such techniques allow differentiating the dynamics of ligand binding. (i) Sharp resonances with negative nOe cross peaks and fast (or intermediate) diffusion coefficients are originating from weakly bound ligands, exchanging fast on the NMR time scale between a free and an entangled state. (ii) Broadened resonances with negative nOe peaks and slow diffusion coefficients are originating from strongly bound ligands, in slow or no exchange with a free species. As the degrees of rotational freedom in the ligand diminish, broadening of resonances increases and signals may become unobservable. As shown here, this is especially so for smaller molecules such as glutamine when compared to, *e.g.*, oleic acid, which has a long aliphatic and mobile tail and remains observable.[10,39,58] However, the introduction of ligands that contain a methyl moiety can alleviate this, thereby allowing monitoring of the bound species in this case. Although some precedence[59,60] exists wherein resonances are assigned to short, bound ligands, solely based on the 1D ^{1}H NMR

spectrum, such practice must be dealt with caution, and further validation using NOESY or DOSY experiments is always desired, especially for short ligands.

Conclusion

We presented a versatile, amino acid based, ligand exchange method to stabilize metal oxide NCs in various polar media. We studied the mechanism of this ligand exchange and found that a strong acid is necessary to protonate the original carboxylic acid ligand, after which a positively charged amino acid adsorbs on the surface, stabilizing the dispersion electrostatically. However, there is a small amount of remaining carboxylic acid on the NC surface which adds a steric contribution to the colloidal stabilization. The amino acids are tightly bound to the surface and their ^{1}H NMR resonances are broadened beyond detection. Nevertheless, we could infer their presence by means of competitive titration experiments or, alternatively, by using amino acids with a methyl moiety. Especially the presence of methyl moieties is most useful for the direct detection of the bound form. These functional groups have a higher internal rotational mobility, which is beneficial for the chance of detecting the bound form of a small ligand, even when it is located relatively close to the surface. DOSY measurements demonstrated that the broad methyl resonance displays the same diffusion coefficient as the nanocrystals and therefore, that the amino acid is tightly bound to the NC surface. We presented here a first exhaustive account on the NMR characterization of short, tightly bound ligands, and found that only through the combination of 1D and 2D DOSY and NOESY techniques the surface chemistry be elucidated. Previously, short molecule binding was only proven in the case of weakly binding ligands using NOESY experiments.[38] The insights developed in this paper will facilitate further research, characterization and development of ligand exchange methods with short ligands.

Acknowledgement

The Research Foundation–Flanders (FWO–Vlaanderen) is thanked for a predoctoral fellowship to J.D.R., a postdoctoral fellowship to D.S., and a research project (G.0760.12) to Z.H. ZH acknowledges the Belgian Science Policy office (IAP 7.35, photonics@be) for funding. K.D.K. thanks BOF for her predoctoral fellowship. JCM thanks the Hercules foundation for funding of the 500 MHz NMR equipment used in this work. IVD and HR thank EUROTAPES, a collaborative project funded by the European Community's Seven Framework Programme (EU–FP7 NMP–LA–2012–280432). The authors thank Johan van der Eycken (Ghent University) for the use of the ATR–FTIR device.

Supporting Information Available

DLS measurements of different oxides, stabilized with different amino acids and TFA or TFSA; ^{1}H NMR measurements of purified dispersions, nonpurified dispersion and the supernatant; ^{1}H NMRmeasurements of HfO_2 NCs with Thr, Met and Leu; 2D NOESY spectrum of HfO_2 NCs with Thr; zero–quantum filtered NOESY of HfO_2 NCs with Gln.

This material is available free of charge via the Internet at `http://pubs.acs.org/`.

References

(1) Kovalenko, M. V.; Manna, L.; Cabot, A.; Hens, Z.; Talapin, D. V.; Kagan, C. R.; Klimov, V. I.; Rogach, A. L.; Reiss, P.; Milliron, D. J.; Guyot-Sionnnest, P.; Konstantatos, G.; Parak, W. J.; Hyeon, T.; Korgel, B. A.; Murray, C. B.; Heiss, W. Prospects of nanoscience with nanocrystals. *ACS Nano* **2015**, *9*, 1012–1057.

(2) Lee, J. S.; Kovalenko, M. V.; Huang, J.; Chung, D. S.; Talapin, D. V. Band–like transport, high electron mobility and high photoconductivity in all–inorganic nanocrystal arrays. *Nat. Nanotechnol.* **2011**, *6*, 348–352.

(3) Tang, J.; Kemp, K. W.; Hoogland, S.; Jeong, K. S.; Liu, H.; Levina, L.; Furukawa, M.; Wang, X. H.; Debnath, R.; Cha, D. K.; Chou, K. W.; Fischer, A.; Amassian, A.; Asbury, J. B.; Sargent, E. H. Colloidal-quantum-dot photovoltaics using atomic–ligand passivation. *Nat. Mater.* **2011**, *10*, 765–771.

(4) Ibáñez, M.; Korkosz, R. J.; Luo, Z.; Riba, P.; Cadavid, D.; Ortega, S.; Cabot, A.; Kanatzidis, M. G. Electron doping in bottom-up engineered thermoelectric nanomaterials through HCl-mediated ligand displacement. *J. Am. Chem. Soc.* **2015**, *137*, 4046–4049.

(5) Schneller, T.; Halder, S.; Waser, R.; Pithan, C.; Dornseiffer, J.; Shiratori, Y.; Houben, L.; Vyshnavi, N.; Majumder, S. B. Nanocomposite thin films for miniaturized multi-layer ceramic capacitors prepared from barium titanate nanoparticle based hybrid solutions. *J. Mater. Chem.* **2011**, *21*, 7953–7965.

(6) Bretos, I.; Schneller, T.; Falter, M.; Backer, M.; Hollmann, E.; Wordenweber, R.; Molina-Luna, L.; Van Tendeloo, G.; Eibl, O. Solution-derived YBa2Cu3O7-[δ] (YBCO) superconducting films with BaZrO3 (BZO) nanodots based on reverse micelle stabilized nanoparticles. *J. Mat. Chem. C* **2015**, *3*, 3971–3979.

(7) Cayado, P.; De Keukeleere, K.; Garzón, A.; Perez-Mirabet, L., Meledin, A.; De Roo, J.; Valles, F.; Mundet, B.; Rijckaert, H.; Pollefeyt, G.; Coll Bau, M.; Ricart, S.; Palau, A.; Gazquez, J.; Ros, J.; Van Tendeloo, G.; Van Driessche, I.; Puig, T.; Obradors, X. Epitaxial YBa2Cu3O7-x nanocomposite thin films from colloidal solutions *Supercond. Sci. Technol.* **2015**, *28*, 124007.

(8) Llordes, A.; Garcia, G.; Gazquez, J.; Milliron, D. J. Tunable near–infrared and visible–light transmittance in nanocrystal-in-glass composites *Nature* **2013**, *500*, 323.

(9) Milliron, D. J.; Buonsanti, R.; Llordes, A.; Helms, B. A. Constructing functional mesostructured materials from colloidal nanocrystal building blocks *Acc. Chem. Res.* **2014**, *47*, 236–246.

(10) De Roo, J.; Van den Broeck, F.; De Keukeleere, K.; Martins, J. C.; Van Driessche, I.; Hens, Z. Unravelling the surface chemistry of metal oxide nanocrystals, the role of acids and bases. *J. Am. Chem. Soc.* **2014**, *136*, 9650–9657.

(11) Grote, C.; Cheema, T. A.; Garnweitner, G. Comparative study of ligand binding during the postsynthetic stabilization of metal oxide nanoparticles. *Langmuir* **2012**, *28*, 14395–14404.

(12) Grote, C.; Chiad, K. J.; Vollmer, D.; Garnweitner, G. Unspecific ligand binding yielding stable colloidal ITO-nanoparticle dispersions. *Chem. Commun.* **2012**, *48*, 1464–1466.

(13) Rudolph, M.; Peuker, U. A. Phase transfer of agglomerated nanoparticles: deagglomeration by adsorbing grafted molecules and colloidal stability in polymer solutions. *Journal of Nanoparticle Research* **2012**, *14*.

(14) Zhou, S. X.; Garnweitner, G.; Niederberger, M.; Antonietti, M. Dispersion behavior of zirconia nanocrystals and their surface functionalization with vinyl group-containing ligands. *Langmuir* **2007**, *23*, 9178–9187.

(15) Pillai, P. P.; Huda, S.; Kowalczyk, B.; Grzybowski, B. A. Controlled pH stability and adjustable cellular uptake of mixed-charge nanoparticles *J. Am. Chem. Soc.* **2013**, *135*, 6392–6395.

(16) Tohgha, U.; Varga, K.; Balaz, M. Achiral CdSe quantum dots exhibit optical activity in the visible region upon post-synthetic ligand exchange with D- or L-cysteine *Chem. Commun.* **2013**, *49*, 1844–1846.

(17) Tosun, B. S.; Chernomordik, B. D.; Gunawan, A. A.; Williams, B.; Mkhoyan, K. A.; Francis, L. F.; Aydil, E. S. Cu2ZnSnS4 nanocrystal dispersions in polar liquids. *Chem. Commun.* **2013**, *49*, 3549–3551.

(18) Liu, W. Y.; Lee, J. S.; Talapin, D. V. III-V Nanocrystals capped with molecular metal chalco-

genide ligands: high electron mobility and ambipolar photoresponse. *J. Am. Chem. Soc.* **2013**, *135*, 1349–1357.

(19) Nag, A.; Kovalenko, M. V.; Lee, J. S.; Liu, W. Y.; Spokoyny, B.; Talapin, D. V. Metal-free inorganic ligands for colloidal nanocrystals: S2-, HS-, Se2-, HSe-, Te2-, HTe-, TeS32-, OH-, and NH2- as Surface Ligands. *J. Am. Chem. Soc.* **2011**, *133*, 10612–10620.

(20) Muro, E.; Pons, T.; Lequeux, N.; Fragola, A.; Sanson, N.; Lenkei, Z.; Dubertret, B. Small and stable sulfobetaine zwitterionic quantum Dots for functional live-cell imaging. *J. Am. Chem. Soc.* **2010**, *132*, 4556.

(21) Kovalenko, M. V.; Scheele, M.; Talapin, D. V. Colloidal nanocrystals with molecular metal chalcogenide surface ligands. *Science* **2009**, *324*, 1417–1420.

(22) Maes, J.; Dierick, R.; Capon, B.; Detavernier, C.; Hens, Z. Se-containing inks for the formation of CuInSe2 films without gas-phase selenization *Solar Energy Materials and Solar Cells* **2016**, *145*, 126–133.

(23) Zhang, H.; Jang, J.; Liu, W. Y.; Talapin, D. V. Colloidal nanocrystals with inorganic halide, pseudohalide, and halometallate Ligands. *ACS Nano* **2014**, *8*, 7359–7369.

(24) Huang, J.; Liu, W. Y.; Dolzhnikov, D. S.; Protesescu, L.; Kovalenko, M. V.; Koo, B.; Chattopadhyay, S.; Shenchenko, E. V.; Talapin, D. V. Surface functionalization of semiconductor and oxide nanocrystals with small inorganic oxoanions (PO43-, MoO42-) and polyoxometalate ligands. *ACS Nano* **2014**, *8*, 9388–9402.

(25) Dirin, D. N.; Dreyfuss, S.; Bodnarchuk, M. I.; Nedelcu, G.; Papagiorgis, P.; Itskos, G.; Kovalenko, M. V. Lead halide perovskites and other metal halide complexes as inorganic capping ligands for colloidal nanocrystals. *J. Am. Chem. Soc.* **2014**, *136*, 6550–6553.

(26) Vilas-Boas, V.; Guldris, N.; Carbo-Argibay, E.; Stroppa, D. G.; Cerqueira, M. F.; Espina, B.; Rivas, J.; Rodriguez-Abreu, C.; Kolen'ko, Y. V. Straightforward phase-transfer route to col-

loidal iron oxide nanoparticles for protein immobilization. *Rsc Advances* **2015**, *5*, 47954–47958.

(27) Palma, S.; Marciello, M.; Carvalho, A.; Veintemillas-Verdaguer, S.; Morales, M. D.; Roque, A. C. A. Effects of phase transfer ligands on monodisperse iron oxide magnetic nanoparticles. *Journal of Colloid and Interface Science* **2015**, *437*, 147–155.

(28) Lin, W.; Walter, J.; Burger, A.; Maid, H.; Hirsch, A.; Peukert, W.; Segets, D. A general approach to study the thermodynamics of ligand adsorption to colloidal surfaces demonstrated by means of catechols binding to zinc oxide quantum dots. *Chem. Mater.* **2014**, *27*, 358–369.

(29) Liu, Y.; Chen, T.; Wu, C. C.; Qiu, L. P.; Hu, R.; Li, J.; Cansiz, S.; Zhang, L. Q.; Cui, C.; Zhu, G. Z.; You, M. X.; Zhang, T.; Tan, W. H. Facile surface functionalization of hydrophobic magnetic nanoparticles. *J. Am. Chem. Soc.* **2014**, *136*, 12552–12555.

(30) Kim, C. S.; Tonga, G. Y.; Solfiell, D.; Rotello, V. M. Inorganic nanosystems for therapeutic delivery: status and prospects. *Adv. Drug Delivery Rev.* **2013**, *65*, 93–99.

(31) Dong, A. G.; Ye, X. C.; Chen, J.; Kang, Y. J.; Gordon, T.; Kikkawa, J. M.; Murray, C. B. A generalized ligand-exchange strategy enabling sequential surface functionalization of colloidal nanocrystals. *J. Am. Chem. Soc.* **2011**, *133*, 998–1006.

(32) Rosen, E. L.; Buonsanti, R.; Llordes, A.; Sawvel, A. M.; Milliron, D. J.; Helms, B. A. Exceptionally mild reactive stripping of native ligands from nanocrystal surfaces by using Meerwein's salt. *Angew. Chem.-Int. Ed.* **2012**, *51*, 684–689.

(33) Doris, S. E.; Lynch, J. J.; Li, C. Y.; Wills, A. W.; Urban, J. J.; Helms, B. A. Mechanistic insight into the formation of cationic naked nanocrystals generated under equilibrium control. *J. Am. Chem. Soc.* **2014**, *136*, 15702–15710.

(34) Niederberger, M.; Garnweitner, G.; Krumeich, F.; Nesper, R.; Colfen, H.; Antonietti, M.

Tailoring the surface and solubility properties of nanocrystalline titania by a nonaqueous in situ functionalization process. *Chem. Mater.* **2004**, *16*, 1202–1208.

(35) Gholami, A.; Rasoul-amini, S.; Ebrahiminezhad, A.; Seradj, S. H.; Ghasemi, Y. Lipoamino acid coated superparamagnetic iron oxide nanoparticles concentration and time dependently enhanced growth of human hepatocarcinoma cell line (Hep-G2). *Journal of Nanomaterials* **2015**

(36) Selvakannan, P. R.; Mandal, S.; Phadtare, S.; Pasricha, R.; Sastry, M. Capping of gold nanoparticles by the amino acid lysine renders them water-dispersible. *Langmuir* **2003**, *19*, 3545–3549.

(37) Sousa, M. H.; Rubim, J. C.; Sobrinho, P. G.; Tourinho, F. A. Biocompatible magnetic fluid precursors based on aspartic and glutamic acid modified maghemite nanostructures. *Journal of Magnetism and Magnetic Materials* **2001**, *225*, 67–72.

(38) Kollath, V. O.; Van den Broeck, F.; Feher, K.; Martins, J. C.; Luyten, J.; Traina, K.; Mullens, S.; Cloots, R. A Modular Approach To Study Protein Adsorption on Surface Modified Hydroxyapatite. *Chemistry-a European Journal* **2015**, *21*, 10497–10505.

(39) De Roo, J.; Justo, Y.; De Keukeleere, K.; Van den Broeck, F.; Martins, J. C.; Van Driessche, I.; Hens, Z. Carboxylic-acid-passivated metal oxide nanocrystals: ligand exchange characteristics of a new binding motif. *Angew. Chem.-Int. Ed.* **2015**, *54*, 6488–6491.

(40) Lauria, A.; Villa, I.; Fasoli, M.; Niederberger, M.; Vedda, A. Multifunctional role of rare earth doping in optical materials: nonaqueous sol-gel synthesis of stabilized cubic HfO2 luminescent nanoparticles. *ACS Nano* **2013**, *7*, 7041–7052.

(41) Ambrosio, R.; Arciniega, O.; Carrillo, A.; Moreno, M.; Heredia, A.; Martinez, C. Organic-inorganic hybrid thin films based in HfO2 nanoparticles as dielectric for flexible electronics. *Can. J. Phys.* **2014**, *92*, 806–812.

(42) Molina, J.; Munoz, A. L.; Calleja, W.; Rosales, P.; Torres, A. High-quality spin-on glass-based oxide as a matrix for embedding HfO2 nanoparticles for metal-oxide-semiconductor capacitors. *J. Mater. Sci.* **2012**, *47*, 2248–2255.

(43) Maggiorella, L.; Barouch, G.; Devaux, C.; Pottier, A.; Deutsch, E.; Bourhis, J.; Borghi, E.; Levy, L. Nanoscale radiotherapy with hafnium oxide nanoparticles. *Future Oncol.* **2012**, *8*, 1167–1181.

(44) Anderson, N. C.; Hendricks, M. P.; Choi, J. J.; Owen, J. S. Ligand exchange and the stoichiometry of metal chalcogenide nanocrystals: spectroscopic observation of facile metal-carboxylate displacement and binding. *J. Am. Chem. Soc.* **2013**, *135*, 18536–18548.

(45) Cros-Gagneux, A.; Delpech, F.; Nayral, C.; Cornejo, A.; Coppel, Y.; Chaudret, B. Surface chemistry of InP quantum Dots: a comprehensive study. *J. Am. Chem. Soc.* **2010**, *132*, 18147–18157.

(46) Valdez, C. N.; Schimpf, A. M.; Gamelin, D. R.; Mayer, J. M. Low capping group surface density on zinc oxide nanocrystals. *ACS Nano* **2014**, *8*, 9463–9470.

(47) Protesescu, L.; Nachtegaal, M.; Voznyy, O.; Borovinskaya, O.; Rossini, A. J.; Emsley, L.; Coperet, C.; Gunther, D.; Sargent, E. H.; Kovalenko, M. V. Atomistic description of thiostannate-capped CdSe nanocrystals: retention of four-coordinate SnS4 motif and preservation of Cd-rich stoichiometry. *J. Am. Chem. Soc.* **2015**, *137*, 1862–1874.

(48) Morris-Cohen, A. J.; Frederick, M. T.; Lilly, G. D.; McArthur, E. A.; Weiss, E. A. Chemical, structural, and quantitative analysis of the ligand shells of colloidal quantum Dots. *J. Phys. Chem. Lett.* **2010**, *1*, 1078–1081.

(49) De Roo, J.; De Keukeleere, K.; Feys, J.; Lommens, P.; Hens, Z.; Van Driessche, I. Fast, microwave-assisted synthesis of monodisperse HfO2 nanoparticles. *J. Nanopart. Res.* **2013**, *15*, 1778.

(50) De Keukeleere, K.; De Roo, J.; Lommens, P.; Martins, J. C.; Van der Voort, P.; Van Driessche, I. Fast and tunable synthesis of ZrO2 nanocrystals: mechanistic insights into precursor dependence. *Inorg. Chem.* **2015**, *54*, 3469–3476.

(51) Thrippleton, M. J.; Keeler, J. Elimination of zero-quantum interference in two-dimensional NMR spectra *Angew. Chem.-Int. Ed.* **2003**, *42*, 3938–3941.

(52) Connell, M. A.; Bowyer, P. J.; Bone, P. A.; Davis, A. L.; Swanson, A. G.; Nilsson, M.; Morris, G. A. Improving the accuracy of pulsed field gradient NMR diffusion experiments: Correction for gradient non-uniformity. *J. Magn. Reson.* **2009**, *198*, 121–131.

(53) Sinnaeve, D. The Stejskal-Tanner equation generalized for any gradient shape-an overview of most pulse sequences measuring free diffusion. *Concept Magnetic Res.* **2012**, *40A*, 39–65.

(54) Gomes, R.; Hassinen, A.; Szczygiel, A.; Zhao, Q. A.; Vantomme, A.; Martins, J. C.; Hens, Z. Binding of phosphonic acids to CdSe quantum Dots: a solution NMR study. *Journal of Physical Chemistry Letters* **2011**, *2*, 145–152.

(55) Bogdan, N.; Vetrone, F.; Ozin, G. A.; Capobianco, J. A. Synthesis of ligand-free colloidally stable water dispersible brightly luminescent lanthanide-doped upconverting nanoparticles. *Nano Lett.* **2011**, *11*, 835–840.

(56) Hens, Z.; Martins, J. C. A solution NMR toolbox for characterizing the surface chemistry of colloidal nanocrystals. *Chem. Mater.* **2013**, *25*, 1211–1221.

(57) Fritzinger, B.; Moreels, I.; Lommens, P.; Koole, R.; Hens, Z.; Martins, J. C. In situ observation of rapid ligand exchange in colloidal nanocrystal suspensions using transfer NOE nuclear magnetic resonance spectroscopy. *J. Am. Chem. Soc.* **2009**, *131*, 3024–3032.

(58) Fritzinger, B.; Capek, R. K.; Lambert, K.; Martins, J. C.; Hens, Z. Utilizing self-exchange to address the binding of carboxylic acid ligands to CdSe quantum dots. *J. Am. Chem. Soc.* **2010**, *132*, 10195–10201.

(59) Bonitatibus, P. J.; Torres, A. S.; Kandapallil, B.; Lee, B. D.; Goddard, G. D.; Colborn, R. E.; Marino, M. E. Preclinical assessment of a zwitterionic tantalum oxide nanoparticle X-ray contrast agent. *ACS Nano* **2012**, *6*, 6650–6658.

(60) Schrader, I.; Warneke, J.; Backenkohler, J.; Kunz, S. Functionalization of platinum nanoparticles with L-proline: simultaneous enhancements of catalytic activity and selectivity. *J. Am. Chem. Soc.* **2015**, *137*, 905–912.

Graphical TOC Entry